Adsorption and catalysis on Pt and Pd monolayer-modified Pt single crystal electrodes

Chen, X.

Cover Page

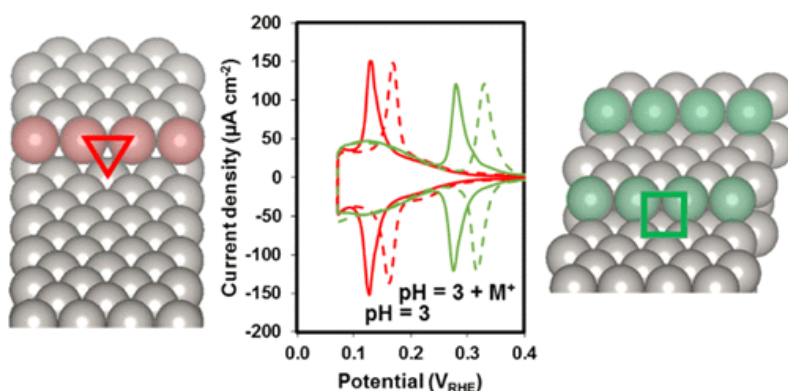## Universiteit Leiden

Author: Chen, X.
Title: Adsorption and catalysis on Pt and Pd monolayer-modified Pt single crystal electrodes
Issue Date: 2019-12-05

3

Effect of Step Density and Orientation on the Apparent pH Dependence of Hydrogen and Hydroxide Adsorption on Stepped Platinum Surfaces

Abstract: *The effect of the alkali-metal cation (Li^+, Na^+, K^+, and Cs^+) on the non-Nernstian pH shift of the Pt(554) and Pt(533) step-associated voltammetric peak is elucidated over a wide pH window (1-13), through computation and experiment. In conjunction with our previously reported study on Pt(553), the non-Nernstian pH shift of the step-induced peak is found to be independent of the step density and the step orientation. In our prior work, we explained the sharp peak as due to the exchange between adsorbed hydrogen and hydroxyl along the step and the non-Nernstian shift as a result of the adsorption of an alkali-metal cation and its subsequent weakening of hydroxyl adsorption. Our density functional theory results support this same mechanism on Pt(533) and capture the effect of alkali-metal cation identity and alkali cation coverage well, where increasing electrolyte pH and cation concentration leads to increased cation coverage and a greater weakening effect on hydroxide adsorption. This chapter paints a consistent picture for the mechanism of these effects, expanding our fundamental understanding of the electrode/electrolyte interface and practical ability to control hydrogen and hydroxyl adsorption thermodynamics via the electrolyte composition, important for improving fuel cell and electrolyzer performance.*

3.1 Introduction

Hydrogen and hydroxyl are important surface-bonded intermediates during many reactions in advanced energy conversion systems, in particular hydrogen evolution, hydrogen oxidation, oxygen evolution, oxygen reduction, and the oxidation of small organic molecules[1-4]. Platinum acts as a remarkable catalyst for these reactions. Therefore, the interactions between the platinum surface and the reacting species attract frequent study[3-5]. Especially, the detailed structure and composition of the electrode/electrolyte interface have a direct effect on the rate and mechanisms of electrocatalytic reactions.

The voltammetric peak associated with the adsorption of hydrogen on step and defect sites, as measured by cyclic voltammograms on stepped platinum and polycrystalline platinum, exhibits anomalous non-Nernstian shifts with pH[6,7]. We have argued previously that the step-related voltammetric peak is due to the replacement of H with OH rather than only ad- or desorption of H[6]. However, within this model, an open question remained whether the non-Nernstian pH dependence of the peak is caused by a residual noninteger charge on adsorbed water[8] or by the co-adsorption of electrolyte cations with adsorbed OH in the step[9,10]. The experimental results cannot be explained by a pH-dependent binding energy of H to step sites[11,12], as the location of the step-associated peak on Pt(553) is independent of pH on a reversible hydrogen electrode (RHE) scale, in the absence of alkali-metal cations in the electrolyte (between pH 0 and 3)[13]. Strmcnik *et al.* previously suggested that the interaction of an alkali-metal cation in the double layer with adsorbed OH was responsible for the experimentally measured cation effects on reactions, which involved adsorbed OH, including oxygen reduction and methanol oxidation[14]; however, they proposed that the alkali-metal cation does not adsorb and remains in the double layer[15]. More recently, based on a detailed comparison between experiments and density functional theory (DFT) calculations of a stepped single-crystal Pt(553) electrode, we showed that the non-Nernstian pH dependence is mediated by the presence of alkali-metal cations adsorbed along the step and their effect on OH adsorption[13].

To demonstrate the generality of this conclusion, here we examine the applicability of this model by reporting and discussing the influence of two relevant parameters on the non-Nernstian pH dependence of the step-related peak, namely the effect of step density and step orientation. Accordingly, we report a combined experimental and computational study on Pt(554) and Pt(533) electrodes. The Pt(554) is a surface consisting of *10*-atom wide terraces of (111) orientation and steps of (110) orientation, whereas the Pt(533) surface consists of four-atom wide terraces of (111) orientation and steps of (100) orientation, allowing us to examine the effects of step density and step orientation, resp.

3.2 Material and Methods

3.2.1 Experimental Details

Electrolytes were made from ultrapure water (Milli-Q, 18.2 MΩ cm), high purity reagents NaOH (99.995%), LiOH (99.995%), KOH (99.99%), CsOH (99.95%), $LiClO_4$ (99.99%) and $CsClO_4$ (99.995%) from Aldrich Ultrapure and $HClO_4$ (70%), H_2SO_4 (96%), $NaClO_4$ (99.99%) and $KClO_4$ (99.99%) from Merck Suprapur. Before each experiment, the electrolytes were first purged with argon (Air Products, 5.7) for at least 30 min to remove air from the solution. Additionally, a trap with KOH (3 M) was used to remove impurities from all the gases before introducing the gases into the cell. Certain commercial materials are identified in this chapter to foster understanding. Such identification does not imply recommendation or endorsement by the National Institute of Standards and Technology, nor does it imply that the materials or equipment identified are necessarily the best available for the purpose.

Cyclic voltammetric measurements were carried out in standard one-compartment electrochemical cells using a three-electrode assembly at room temperature. Experiments were performed in a fluorinated ethylene propylene (PEP, Nalgene) electrochemical cell for alkaline solutions, whereas a glass cell was used for acidic electrolytes. All glassware was cleaned in an acidic solution of potassium permanganate overnight, followed by rinsing with an acidic solution of hydrogen peroxide and repetitive rinsing and boiling with ultrapure water. Stepped single crystal platinum electrodes of (554) and (533) orientation, with surface areas of 2.72 and 4.02 mm^2, resp., were used as the working electrodes. Prior to every experiment, the working electrode was prepared according to the Clavilier method[16]. A platinum wire was used as counter electrode, and a reversible hydrogen electrode (RHE) was employed as the reference electrode, in a separate compartment filled with the same electrolyte, at the same pH as the electrolyte in the electrochemical cell. The electrochemical measurements were performed with the single-crystal electrode in the hanging meniscus configuration. The potential was controlled with an Autolab PGSTAT302N potentiostat. The resistance of the cell was determined before every experiment, and the ohmic drop was compensated accordingly. The current density shown in the manuscript represents the measured current normalized to the geometric area of the working electrode.

3.2.2 Computational Details

The thermodynamics of adsorption of hydrogen, hydroxide, water, and alkali-metal cations along the step of the Pt(533) surface were examined using density functional theory. Simulations were performed using the Vienna ab initio simulations Package[17-19], with a plane wave basis set (with an energy cutoff of 450 eV) and the Perdew-Wang (PW91)[20] exchange-correlation functional. The projector augmented wave approach was used to model the ion core potentials[21,22]. The structural optimization was performed until the forces on the atoms were below 0.02 eV/Å (0.2 eV/nm).

The Pt(553) surface was represented with a 4-layer slab, with the bottom two layers frozen at the experimentally measured Pt lattice constant, 3.92 Å[23]. All simulations were performed in a 1 x 3, 1 x 4, or 1 x 6 unit cell (with 3, 4, or 6 step atoms, resp.), with k-space sampled by a 7 x 7 x 1 (for the 1 x 3 and 1 x 4 unit cells) or 3 x 5 x 1 (for the 1 x 6 unit cell) Monkhorst-Pack[24] mesh grid. Dipole corrections[25] were applied in the surface-normal direction (VASP keywords: IDIPOL=3, LDIPOL=TRUE).

Adsorption of hydrogen was examined at 1 monolayer (ML) and hydroxyl adsorption at 1/6, 1/4, and 1/3 ML (in both the 1 x 3 and 1 x 6 unit cells). Monolayer coverage is defined relative to the number of step atoms (not total surface atoms). Alkali-metal cation (Li, Na, K, and Cs) adsorption along the step was modeled at 1/6 and 1/3 ML (again in both the 1 x 3 and 1 x 6 unit cells). To approximate the effects of near surface solvation, the hydrogen covered step, both with and without a co-adsorbed alkali-metal cation, was solvated by 1 ML of hydrogen-bonded water molecules in a "single-stranded" structure. Adsorbed hydroxyl, in the absence and presence of co-adsorbed alkali-metal cations, was solvated by co-adsorbing water molecules on the step with the hydroxyl, as well as next to the step edge, forming a "double-stranded" structure. We found previously that these water structures gave reasonable step-associated peak potentials for adsorption of hydrogen and hydroxyl along the step of the Pt(553) surface[13]. The use of a single, static water structure is intended only as an approximation of the effects of near-surface solvent on adsorption of hydrogen, hydroxyl, and alkali-metal cations. Images of these structures are given in the Supplementary Information for Chapter 3. Images of the adsorbate structures were rendered with VESTA[26].

Adsorption free energies and the potential of hydrogen/hydroxyl exchange along the step ("step-associated peak potential", referring to the peak in current measured experimentally by cyclic voltammetry associated with adsorption on step sites) are calculated following the methods that we have described previously[10,13]. To expand on our work on Pt(553) in Chapter 2, we have examined

adsorption of hydrogen and hydroxyl in the presence of varying coverages of Li, Na, K, and Cs on the 100-type step of Pt(533).
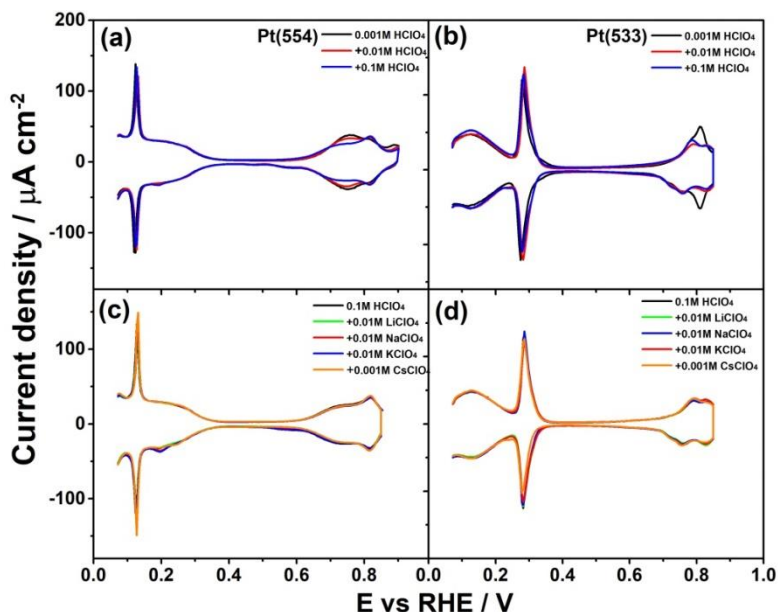
3.3 Results and Discussion

Figure 3.1 Cyclic voltammograms of Pt(554) recorded in (a) 0.1 M HClO$_4$ (pH 1), 0.01 M HClO$_4$ (pH 2), and 0.001 M HClO$_4$ (pH 3), (c) 0.1 M HClO$_4$ (pH 1) with 0.01 M LiClO$_4$, NaClO$_4$, and KClO$_4$ and 0.001 M CsClO$_4$, and (b, d) the same for Pt(533). Scan rate: 50 mV s^{-1}.

Figure 3.1a and b show cyclic voltammograms for the Pt(554) and Pt(533) electrodes in 0.1 M HClO$_4$ (pH 1), 0.01 M HClO$_4$ (pH 2), and 0.001 M HClO$_4$ (pH 3) electrolytes. Voltammograms and peak potentials measured in acidic media on single crystals with varying step density and orientation are typically reproducible and reversible. From the cyclic voltammogram of the Pt(554) electrode in Figure 3.1a, we find three main features: a broad H adsorption-desorption feature attributed to the (111) terrace (0.05<E<0.35 V$_{RHE}$), a (110) step-induced peak involving the replacement of H by OH (E=0.125 V$_{RHE}$), and an adsorption-desorption peak for OH on (111) terraces (0.60<E<0.85 V$_{RHE}$). There is no pH or ionic strength effect on the (110) step-induced peak, which is consistent with our previous study[13]. There is either a slight pH or an anion (ClO$_4^-$) effect on the OH adsorption-desorption feature on terraces, which may be due to the interaction of perchlorate with the OH adlayer[27]. Figure 3.1b shows cyclic voltammograms measured on Pt(533), with (100) step geometry, under the same experimental conditions. When comparing Figure 3.1b to 1a, we observe that the introduction of (100) steps into the (111) surface leads to the step-induced voltammetric peak appearing at more positive potential (E=0.285 V$_{RHE}$), which is in good agreement with a previous report[2]. Strikingly, we observe no effect of

pH or ionic strength on the (110) or (100) step-induced peaks. This rules out the cause of previously observed pH shifts of these peaks being due to a residual noninteger charge on adsorbed water[8].

Figure 3.1c and d show the voltammetric profiles of the Pt(554) and Pt(533) electrodes recorded in 0.1 M $HClO_4$ containing 0.01 M $LiClO_4$, $NaClO_4$, and $KClO_4$ and 0.001 M $CsClO_4$. As we previously found the apparent pH dependence arises from the weakening of hydroxide adsorption along the step edge due to alkali-metal cation adsorption[13], the effect of pH on cation adsorption must be considered. The determination of fundamental properties related to ion adsorption is made by referring to the local potential of zero charge (PZC) measured in the solution with the same pH. The study of the PZC of stepped platinum surfaces vicinal to Pt(111) reveals a marked decrease of the PZC due to the introduction of surface steps[28]. Here, the approximate PZC of the stepped surface is estimated to be 0.2-0.3 V more negative than the 0.3 V_{RHE} value of Pt(111) at a pH 1 (based on measurements on similar stepped surfaces[28]), so approximately 0.0-0.1 V_{RHE}. We assume a similar shift for the Pt(533) surface, though it may be larger due to the higher step density. Therefore, the PZC of a stepped Pt surface at pH 1 suggests that alkali-metal cations would not be specifically adsorbed in the H/OH adsorption region at low pH[13]. As shown in Figure 3.1c and d, the step-induced voltammetric peak is unaffected by the nature of the cation at this pH. Values for the peak potentials are given in Table B.1 in the Supplementary Information for Chapter 3.

However, as the electrolyte pH is increased, hydrogen and hydroxide adsorption shifts to lower absolute potentials (or equivalently the PZC shifts to more positive potentials on the RHE scale), into the region where alkali-metal cation specific adsorption along the Pt step becomes favorable. The left panel of Figure 3.2 shows the voltammetric profiles of the Pt(554) electrode recorded in 0.001 M $HClO_4$ (pH 3) electrolytes containing Li^+, Na^+, K^+, and Cs^+. It shows that with increasing concentration of alkali-metal cation, the (110) step-induced voltammetric peak is shifted to more positive potential in comparison with the peak potential in $HClO_4$ (0.125 V_{RHE}). The shift is more pronounced for larger cations: for 0.01 M Li^+ (Figure 3.2a), Na^+ (Figure 3.2b), K^+ (Figure 3.2c), and Cs^+ (Figure 3.2d) containing electrolytes, the (110) step-induced voltammetric peak is shifted to 0.145, 0.149, 0.153, and 0.163 V_{RHE}, resp. The right panel of Figure 3.2 shows the voltammetric profiles of the Pt(533) electrode under identical experimental conditions. The shift of the (100) step-induced voltammetric peak shows the same trend as the (110) step. The shift is more apparent for larger cations: in 0.01 M Li^+ (Figure 3.2e), Na^+ (Figure 3.2f), K^+ (Figure 3.2g), and Cs^+ (Figure 3.2h) containing electrolytes, the (100) step-induced voltammetric peak is shifted to 0.307, 0.312, 0.315, and 0.324 V_{RHE}, resp.

All values in Figure 3.2 were derived from the step-induced voltammetric peak potentials during the forward scan and summarized in Table B.1. The step-induced voltammetric peak exhibits a

non-Nernstian shift at pH values above 3, illustrating an apparent pH effect as well as an effect of the identity and concentration of the alkali cation. Additionally, increasing the cation concentration at low pH leads to a greater shift in the step-induced voltammetric peak, as shown in Figure 3.2.
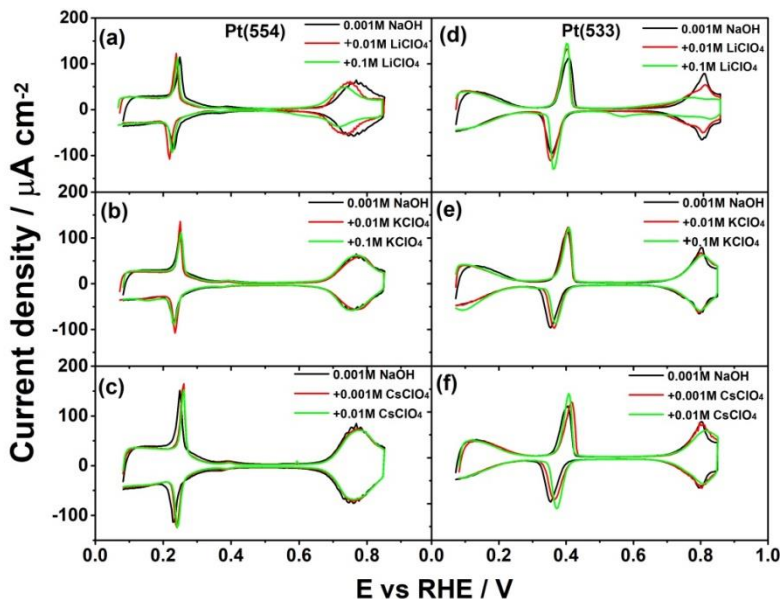

Figure 3.2 Cyclic voltammograms of Pt(554) (a-d) and Pt(533) (e-h) recorded in 0.001 M HClO$_4$ (pH 3) with (a, e) 0.01 and 0.1 M LiClO$_4$, (b, f) 0.01 and 0.1 M NaClO$_4$, (c, g) 0.01 and 0.1 M KClO$_4$, and (d, h) 0.001 and 0.01 M CsClO$_4$. The blank voltammograms for the Pt(554) and Pt(533) recorded in 0.001 M HClO$_4$ (black lines) are shown for comparison. Scan rate: 50 mV s^{-1}.

To confirm that this peak shift is caused by the alkali cation and not related to the anion, similar experiments were performed in 0.0005 M H$_2$SO$_4$ (pH 3). Figure B.1a and b in the Supplementary Information for Chapter 3 show that the step-induced voltammetric peak in the SO$_4^{2-}$ containing electrolytes follows the identical trend as in the presence of ClO$_4^-$, confirming that the shift of the (110) and (100) step-induced voltammetric peaks at 0.125 and 0.285 V$_{RHE}$, resp., is a result of the presence of co-adsorbed cations.

Figure 3.3 shows that with increasing size of alkali-metal cation at pH 11, the (110) step-induced voltammetric peak is shifted to 0.240, 0.248, and 0.260 V$_{RHE}$ for Li$^+$ (Figure 3.3a), K$^+$ (Figure 3.3b), and Cs$^+$ (Figure 3.3c), resp. (as compared to 0.125 V$_{RHE}$ at pH 1). The trend presented above is independent of step orientation, as we find, at pH 11, that the (100) step-induced voltammetric peak is shifted to 0.397, 0.405, and 0.416 V$_{RHE}$ for Li$^+$ (Figure 3.3e), K$^+$ (Figure 3.3f), and Cs$^+$ (Figure 3.3g), resp. (as compared to 0.285 V$_{RHE}$ at pH 1). Figure 3.3d and h also compares the voltammograms of the Pt(554) and Pt(533) electrodes observed in different alkali electrolytes at pH 13. The corresponding

values for the (110) step-induced voltammetric peak potential obtained in 0.1 M LiOH, NaOH, KOH, and CsOH are 0.240, 0.264, 0.269, and 0.291 V_{RHE}, resp. Figure 3.3h shows that in the presence of Li^+, Na^+, and K^+, the (100) step-induced voltammetric peak is at 0.398, 0.403, and 0.428 V_{RHE}, resp. The voltammogram for the (100) step in 0.1 M CsOH is not shown, as it indicates contributions from contamination, a consequence of the CsOH being less pure than that of the other electrolytes. The increasing shift in the step-associated peak with increasing pH is summarized in Figure 3.4, which also highlights how the effect of cation identity becomes apparent at pH≥3.
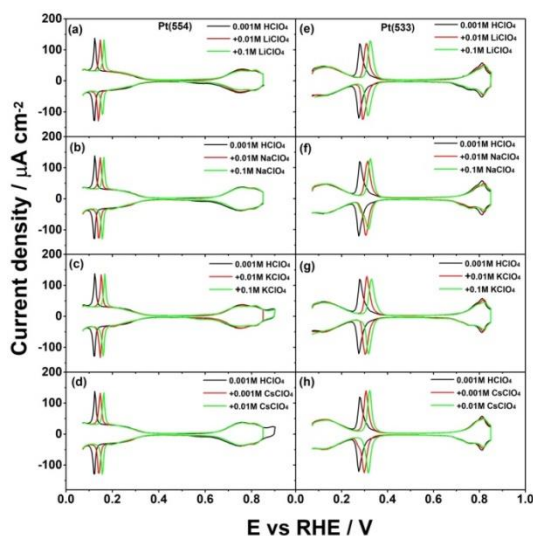

Figure 3.3 Cyclic voltammograms of Pt(554) (a-c) and Pt(533) (e-g) recorded in 0.001 M NaOH (pH 11) with (a, e) 0.01 and 0.1 M LiClO₄, (b, f) 0.01 and 0.1 M KClO₄, and (c, g) 0.001 and 0.01 M CsClO₄. The blank voltammograms for the Pt(554) and Pt(533) recorded in 0.001 M NaOH (black lines) are shown for comparison. Voltammograms of (d) Pt(554) and (h) Pt(533) recorded at pH 13 in 0.1 M MeOH, where Me is Li, Na, K, or Cs, as indicated. Scan rate: 50 mV s⁻¹.
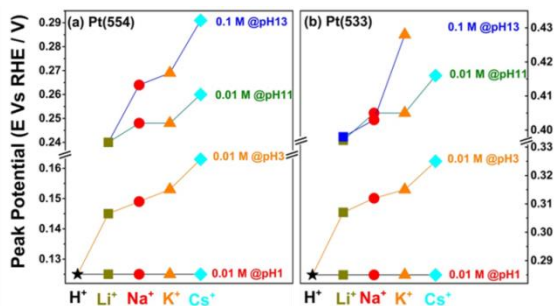

Figure 3.4 Cation dependence of the (a) (110) and (b) (100) step-induced voltammetric peaks at various pH, 0.01 M@pH 3 means 0.01 mol/L cation concentration at pH 3. Peak potential determined in the positive-going scan.

Following our previous work with the Pt(553) surface with the 110-type steps, we used density functional theory to examine the specific adsorption of hydrogen, hydroxide, water, and alkali cations to the 100-type steps of the Pt(533) surface. As the behavior of the stepped surface is relatively independent of terrace width, as shown here (Figure B.2) comparing the Pt(554) surface with Pt(553) in Chapter 2[13], we did not examine the behavior of the Pt(554) surface with DFT.
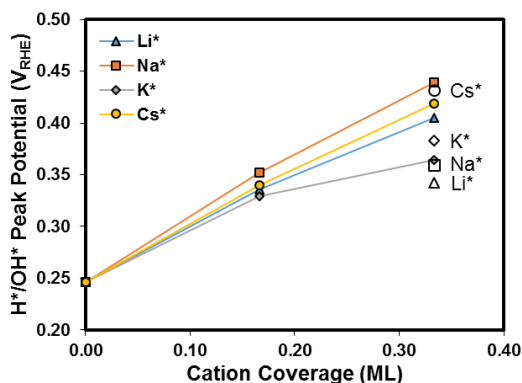

Figure 3.5 Peak potential from DFT calculations for the desorption (adsorption) of H* (at 1 ML) and adsorption (desorption) of OH* (at 1/6 ML in the 1×6 unit cell (colored points) and 1/3 ML in the 1×3 unit cell (empty points)) on the step of Pt(533) plotted as a function of the coverage of co-adsorbed alkali-metal cation adsorbed along the step (Li*, Na*, K*, and Cs*). Lines are intended only as a guide for the eye.

Similar to the Pt(553) surface, we find that the sharp peak associated with adsorption on the 100 step of the Pt(533) surface corresponds to the exchange of adsorbed hydrogen and hydroxide. As the adsorption energy of hydrogen is relatively independent of its coverage on this step[10], we expect 1 ML of hydrogen to be replaced by 1/6 ML of adsorbed hydroxyl, as the potential is shifted positive. The lowest energy hydroxyl coverage that we have identified in the absence of co-adsorbed alkali-metal cations is 1/6 ML (Figure B.3). As the electrolyte pH is increased and an alkali-metal cation is added to the electrolyte solution, adsorption of the alkali-metal cation at the step edge becomes favorable, with an increasing coverage of cation becoming favorable with lower absolute potential (higher pH)[13]. To examine the effects of solvation near the electrode surface, we examined hydrogen adsorption in the presence of water molecules adsorbed next to the step edge, hydrogen bonded in the single-stranded water structure, and hydroxide adsorption with co-adsorbed water molecules in the double-stranded water structure[29]. These structures were identified previously to give adsorption potentials that compare well with experiment for adsorption on the Pt(553) surface[13]. This work goes beyond our prior examination with DFT of adsorption on the Pt(533) surface[10], and we now more fully solvate the step edge and examine lower coverages of adsorbed hydroxyl and adsorbed cation, such that we can examine cation coverages present at intermediate pH. Images of example structures with and without co-adsorbed cations are given in the Supplementary Information for Chapter 3 (Figure B.4 and 5).

Figure 3.5 shows that the presence of an alkali-metal cation adsorbed along the step edge weakens hydroxide adsorption, shifting the competitive adsorption (H/OH replacement) peak to more positive potentials with increasing alkali-metal cation coverage. The difference among the alkali-metal cations in affecting the binding of this low coverage of hydroxide is small. Figure 3.5 also illustrates that a high coverage of alkali-metal cation (1/3 ML M*) makes the adsorption of a higher hydroxide coverage (1/3 ML) more favorable than low coverage (1/6 ML) adsorption. The higher coverage of hydroxide adsorbed in the presence of increasing cation coverage may explain the increase in total charge transferred in the step-associated peak with increasing pH (Figure B.6).
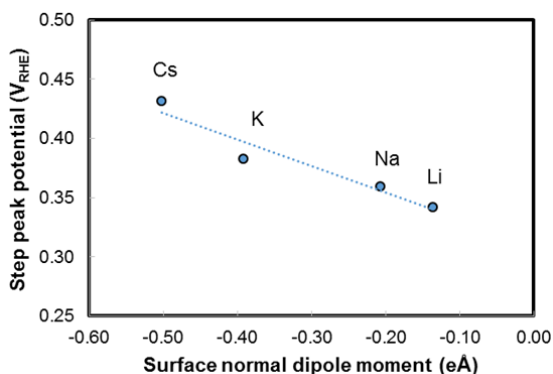

Figure 3.6 Step-associated peak potential (potential where the change in free energy to desorb (adsorb) 1 ML H* and adsorb (desorb) 1/3 ML OH* is equal to zero) plotted as a function of the surface-normal dipole moment for Li*, Na*, K*, and Cs* adsorbed along the step of Pt(533) at 1/3 ML, co-adsorbed with 1 ML H* and 1 ML H_2O* (in the single-stranded structure).

At an adsorbed cation coverage of 1/3 ML and an adsorbed hydroxyl coverage of 1/3 ML (the most favorable coverages in a high pH electrolyte), there is a clear trend among the cations in the magnitude of the weakening of hydroxide adsorption. Compared to 1/6 ML OH* at low pH in the absence of adsorbed cation, Li* shows the smallest weakening effect, and Cs* shows the largest effect. Similar to our findings at the Pt(553) surface, we find that this trend correlates with the trend in retained charge on the adsorbed cation, which is proportional to the change in surface-normal dipole moment on adsorption of the cation (Figure 3.6). The trend in the effect of the cations on hydroxide adsorption also correlates with the ionic radius of the cations (following Li<Na<K<Cs), though the ionic radius may be altered on adsorption due to electron transfer with the surface. The size of the adsorbed cation may directly affect how co-adsorbed water forms hydrogen bonds with adsorbed hydroxyl. Further, the charge retained on the cation and its ionic radius when adsorbed determine the electrostatic field exerted by the adsorbed cations on co-adsorbed or near-surface water and adsorbed hydroxyl. The presence of the co-adsorbed cations drives water dipoles to reorient and alters the OH* + H_2O* structure[9], which will be discussed shortly. The cations which retain a greater amount of positive charge

on adsorption (yielding a more negative surface-normal dipole moment), cause a greater disruption of the hydrogen bonding between co-adsorbed hydroxide and water[9], resulting in weaker hydroxide adsorption, and a shift in the step-associated peak to more positive potentials.

Comparing these results directly to experiment, Figure 3.7 plots the DFT-calculated potential corresponding to competitive H*/OH* adsorption on the (100) step of the Pt(533) surface with that experimentally measured as a function of pH and cation concentration. Figure 3.7 also includes the DFT calculated and experimentally measured peak potential for the 110 step of the Pt(553) surface from Chapter 2.

For the Pt(533) surface, the data in Figure 3.7 include the peak potential measured in an acid electrolyte (pH 1) in the absence of an alkali-metal cation, measured in a pH 3 electrolyte in the presence of 0.01 M M^+ (where M^+ = Li^+, Na^+, K^+, and Cs^+), and measured in a pH 13 electrolyte at 0.1 M M^+ (where M^+ = Li^+, Na^+, and K^+). As cation specific adsorption becomes more favorable with increasing cation concentration and increasing pH (relative to H/OH adsorption on a relative hydrogen electrode scale), a higher cation coverage (1/3 ML) is favorably adsorbed in high pH electrolytes (pH 13) and a lower coverage (1/6 ML) in low pH electrolytes (pH 3). Although the investigation of other coverages of both adsorbed hydroxyl and co-adsorbed cation was considered, exhaustive evaluation at a large range of coverages is difficult as separating the cation coverage and hydroxyl coverage requires the use of a large unit cell, where the number of step atoms is a multiple of both the cation and hydroxyl coverages.
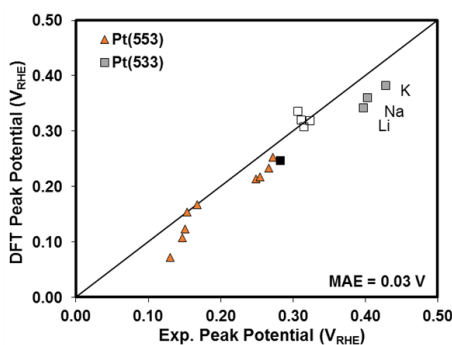

Figure 3.7 DFT-calculated equilibrium potential to exchange 1 ML H* with OH* on the step of the Pt(553) surface[13] (triangles) and the Pt(533) surface (squares) plotted against the experimentally measured potential of the sharp, step-associated peak. The solid black square represents the location of the peak measured at low pH (pH 1-3) in the absence of alkali-metal cations, with a simulated hydroxyl coverage of 1/6 ML. The white squares correspond to potentials measured at pH 3 in the presence of 0.01 mol/L Li, Na, K, and Cs and simulated with a hydroxyl coverage of 1/6 ML and Li, Na, K, or Cs coverage of 1/6 ML. The solid gray squares correspond to potentials measured at pH 13 in 0.1 mol/L LiOH, NaOH, and KOH, with a simulated hydroxyl coverage of 1/3 ML and adsorbed Li, Na, and K coverage of 1/3 ML. The solid black line is y = x, and the calculated mean absolute error is 0.03 V.

The DFT results match experiment well, capturing not only the effect of pH, which leads to an increased coverage of adsorbed cation and a greater weakening of hydroxide adsorption, but also the differences between the identities of the alkali-metal cation (where Li tends to have the smallest effect in weakening hydroxide and Cs the largest). Although not shown in Figure 3.7, this mechanism also explains the increased shift in peak potential with increasing cation concentration (Figure 3.2), which, similar to the effect of pH, would lead to a greater coverage of adsorbed cation and greater weakening of adsorbed hydroxide. The effect of the type of step is also well captured by DFT, with the 100 step of the Pt(533) surface showing weaker hydroxide adsorption (and slightly stronger hydrogen adsorption[30]), in all of the electrolytes examined, than on the (110) step of the Pt(553) surface, leading to a more positive step-associated peak potential. Although the trend between the cations at low pH (pH 3) and low cation concentration (0.01 M) is not captured well by DFT calculations of the Pt(533) surface, the experimentally measured differences between the cations are small under these conditions (span of only 0.017 V). It is important to note that we have considered only one low cation coverage (1/6 ML), we have examined and compared only between cations adsorbed at the same coverage (all at 1/6 ML or all at 1/3 ML), and we have evaluated only a small number of near-surface water structures. The real adsorbed cation coverage under these conditions may be different from 1/6 ML, the cations could each adsorb with different coverages, as the cations exhibit different adsorption thermodynamics, and the water structure may change between the various cations.

Figure 3.7 supports a consistent picture of the role of the alkali-metal cation as the cause of the apparent pH dependence of the step-associated peak, for both 110- and 100-type steps, in adsorbing along the step edge and weakening hydroxyl adsorption. Further, the experimental results on the Pt(554) surface (Figure 3.4a) illustrate that the mechanism of this effect is independent of terrace width, at least for relatively wide terraces, giving similar results to those previously measured on Pt(553)[13].
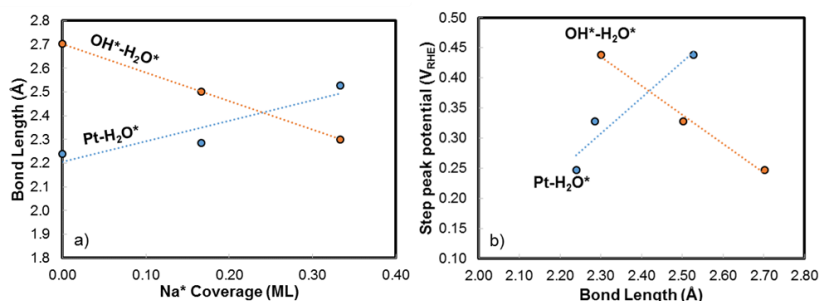

Figure 3.8 (a) Pt-O (blue) and hydrogen bond (orange) lengths between the platinum surface and adsorbed water and between co-adsorbed hydroxyl and water (with OH* as the hydrogen bond donor), resp., as a function of the coverage of sodium co-adsorbed along the step on Pt(533). OH* coverage was 1/6 ML (calculated in 1×6 unit cell). (b) Step-associated peak potential given as a function of the bond lengths shown in (a) (which depend on the Na* coverage).

To further understand the mechanism by which co-adsorbed alkali-metal cations affect hydroxide adsorption, we also examined the change in bonding between the metal surface, hydroxyl, and co-adsorbed water as a function of cation coverage and identity. Figure 3.8a shows that at a low hydroxyl coverage (1/6 ML), the presence of specifically adsorbed Na* along the step edge causes a lengthening of the Pt-O bond between the platinum surface and adsorbed water and a decreasing in length of hydrogen bonds between OH* and H_2O^* (with OH* as the hydrogen bond donor). The change in these bond lengths becomes larger with increasing Na* coverage and correlates with the continuous increase of the step-associated peak potential with increasing Na* coverage (Figure 3.8b). Other changes in the adlayer structure with increasing Na* coverage are given in Figure B.7 (Pt-OH*, H_2O^*-OH*, and H_2O^*-H_2O^* bond lengths).
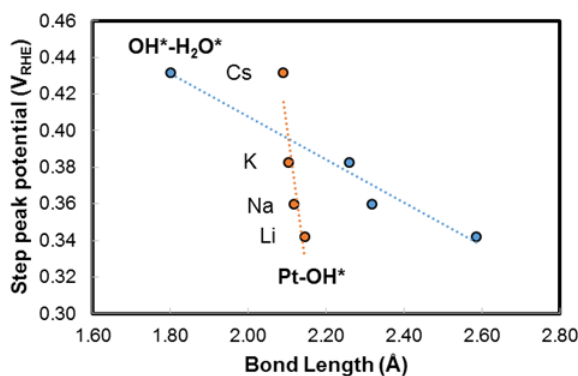

Figure 3.9 Step-associated peak potential calculated at 1/3 ML OH* and 1/3 ML adsorbed alkali-metal cation (Li, Na, K, and Cs) on Pt(533) plotted as a function of the platinum-hydroxyl bond length and the hydroxyl-water hydrogen bond length (between co-adsorbed hydroxyl and water, with hydroxyl as the hydrogen bond donor). Dotted lines are linear regressions of the data, intended only as a guide for the general trend.

Figure 3.9 shows a correlation between the Pt-O bond lengths between the platinum surface and adsorbed OH*, the hydrogen bond length between OH* and H_2O^* (with OH* as the hydrogen bond donor), and the step-associated peak potential in the presence of Li*, Na*, K*, and Cs* at 1/3 ML and OH* at 1/3 ML. Both the platinum-hydroxyl bond length and the hydrogen bond length between OH* and H_2O^* decrease in the order Li>Na>K>Cs, following the trend of increasing peak potential. Although the Pt-O bond length between the platinum surface and adsorbed H_2O^* was dependent on the adsorbed cation coverage, it was relatively independent of cation identity at high coverage (1/3 ML) (not shown). The results in Figures 3.8 and 3.9 show that the weakening of hydroxyl adsorption (indicated by a more positive adsorption potential) is correlated with a decrease in the length of the Pt-O bonds between Pt and hydroxyl and in the hydrogen bonds between OH* and H_2O^*, as well as an increase in length of the Pt-O bond between Pt and H_2O^*. As an increasing bond length between an adsorbate and the surface typically correlates with weaker adsorption, this suggests that the effect of the

adsorbed cation on OH* + H$_2$O* adlayer formation is driven primarily by its weakening of water adsorption, as the positive charge retained by the cation drives a reorientation of water dipoles adsorbed on or near the electrode surface.

3.4 Conclusions

We have used both experiment and density functional theory to understand the effects of electrolyte pH, cation concentration, and cation identity on the step-associated peak in current measured by cyclic voltammetry on Pt(554) and Pt(533), stepped platinum surfaces with the 110- and 100-type steps, resp. Consistent with Chapter 2, we find that this sharp peak corresponds to competitive hydrogen and hydroxyl adsorption onto both types of step sites. Further, we show that this step-associated peak exhibits an apparent anomalous pH dependence, whereas the (111) terrace associated peak does not. As the electrolyte pH is increased, specific adsorption of alkali-metal cations along the steps becomes increasingly favorable. These adsorbed cations retain most of their charge and disrupt hydrogen bonding between co-adsorbed hydroxyl and water along the step. This weakens hydroxyl and water adsorption and shifts the step-associated peak to more positive potentials. The effects of pH, cation concentration, and cation identity on voltammograms measured on Pt(554) match that seen in Chapter 2 with Pt(553) (110-type steps with a four-atom wide terrace), suggesting that the effect is independent of step density, at least for the step densities investigated here. Similar effects are measured on Pt(533), though with the step-associated peak shifted to more positive potentials in all electrolytes investigated, relative to Pt(554). Our DFT results captured the apparent effect of pH, the effect of cation concentration, and cation identity well, as well as the differences between adsorption on the 100- and 110-type steps. The 100-type step binds hydroxyl more weakly and hydrogen slightly more strongly than the 110-type step, explaining why the step-associated peak is shifted to more positive potentials on the Pt(533) surface.

This chapter highlights the importance of the effects of electrolyte composition on the adsorption of hydrogen and hydroxide, reactive intermediates in many electrocatalytic reactions, where the thermodynamics of adsorption have a direct effect on the kinetics and mechanisms of these reactions. This chapter also furthers our fundamental understanding of the electrode/electrolyte interface, tying the structure of the double layer directly to the thermodynamics of adsorption of these species. Additionally, we anticipate that the insights developed here for model, single-crystal 110- and 100-type stepped surfaces can be extended to explain the effects of electrolyte composition on electrocatalysis on more complex surfaces containing these types of sites, such as Pt nanoparticles.

References

1 Marković, N. & Ross Jr, P. Surface science studies of model fuel cell electrocatalysts. *Surf. Sci. Rep.* **45**, 117-229 (2002).

2 Solla-Gullón, J., Rodríguez, P., Herrero, E., Aldaz, A. & Feliu, J. M. Surface characterization of platinum electrodes. *Phys. Chem. Chem. Phys.* **10**, 1359-1373 (2008).

3 Koper, M. T. M. Structure sensitivity and nanoscale effects in electrocatalysis. *Nanoscale* **3**, 2054-2073, (2011).

4 Bandarenka, A. S. & Koper, M. T. M. Structural and electronic effects in heterogeneous electrocatalysis: Toward a rational design of electrocatalysts. *J. Catal.* **308**, 11-24 (2013).

5 Magnussen, O. M. Ordered Anion Adlayers on Metal Electrode Surfaces. *Chem. Rev.* **102**, 679-726 (2002).

6 Van der Niet, M. J., Garcia-Araez, N., Hernández, J., Feliu, J. M. & Koper, M. T. M. Water dissociation on well-defined platinum surfaces: The electrochemical perspective. *Catal. Today* **202**, 105-113 (2013).

7 Gisbert, R., García, G. & Koper, M. T. M. M. Oxidation of carbon monoxide on poly-oriented and single-crystalline platinum electrodes over a wide range of pH. *Electrochim. Acta* **56**, 2443-2449 (2011).

8 Schwarz, K., Xu, B., Yan, Y. & Sundararaman, R. Partial oxidation of step-bound water leads to anomalous pH effects on metal electrode step-edges. *Phys. Chem. Chem. Phys.* **18**, 16216-16223 (2016).

9 McCrum, I. T. & Janik, M. J. pH and Alkali Cation Effects on the Pt Cyclic Voltammogram Explained Using Density Functional Theory. *J. Phys. Chem. C* **120**, 457-471 (2016).

10 McCrum, I. T. & Janik, M. J. First Principles Simulations of Cyclic Voltammograms on Stepped Pt (553) and Pt (533) Electrode Surfaces. *ChemElectroChem* **3**, 1609-1617 (2016).

11 Durst, J., Siebel, A., Simon, C., Hasche, F., Herranz, J., Gasteiger, H. New insights into the electrochemical hydrogen oxidation and evolution reaction mechanism. *Energy Environ. Sci.* **7**, 2255-2260 (2014).

12 Zheng, J., Sheng, W., Zhuang, Z., Xu, B. & Yan, Y. Universal dependence of hydrogen oxidation and evolution reaction activity of platinum-group metals on pH and hydrogen binding energy. *Sci. Adv.* **2**, e1501602 (2016).

13 Chen, X., McCrum, I. T., Schwarz, K. A., Janik, M. J. & Koper, M. T. M. Co-adsorption of Cations as the Cause of the Apparent pH Dependence of Hydrogen Adsorption on a Stepped Platinum Single-Crystal Electrode. *Angew. Chem. Int. Ed.* **56**, 15025-15029 (2017).

14 Strmcnik, D., Kodama, K., van der Vliet, D., Greeley, J., Stamenkovic, V. R. & Marković, N. The role of non-covalent interactions in electrocatalytic fuel-cell reactions on platinum. *Nat. Chem.* **1**, 466 (2009).

15 Strmcnik, D., Van der Vliet, D. F., Chang, K. C., Komanicky, V., Kodama, K., You, H., Stamenkovic, V. R. & Marković, N. M. Effects of Li$^+$, K$^+$, and Ba^{2+} Cations on the ORR at Model and High Surface Area Pt and Au Surfaces in Alkaline Solutions. *J. Phys. Chem. Lett.* **2**, 2733-2736 (2011).

16 Clavilier, J., Armand, D., Sun, S. G. & Petit, M. Electrochemical adsorption behaviour of platinum stepped surfaces in sulphuric acid solutions. *J. Electroanal. Chem. Interfacial Electrochem.* **205**, 267-277 (1986).

17 Kresse, G. & Furthmüller, J. Efficient iterative schemes for ab initio total-energy calculations using a plane-wave basis set. *Phys. Rev. B* **54**, 11169-11186 (1996).

18 Kresse, G. & Furthmüller, J. Efficiency of ab-initio total energy calculations for metals and semiconductors using a plane-wave basis set. *Comput. Mater. Sci.* **6**, 15-50 (1996).

19 Kresse, G. & Hafner, J. Ab initio molecular dynamics for liquid metals. *Phys. Rev. B* **47**, 558-561 (1993).

20 Perdew, J. P., Chevary, J. A., Vosko, S. H., Jackson, K. A., Pederson, M. R., Singh, D. J. & Fiolhais, C. Atoms, molecules, solids, and surfaces: Applications of the generalized gradient approximation for exchange and correlation. *Phys. Rev. B* **46**, 6671-6687 (1992).

21 Blöchl, P. E. Projector augmented-wave method. *Phys. Rev. B* **50**, 17953-17979 (1994).

22 Kresse, G. & Joubert, D. From ultrasoft pseudopotentials to the projector augmented-wave method. *Phys. Rev. B* **59**, 1758-1775 (1999).

23 Kittel, C. Introduction to solid state physics. Vol. 8 (wiley Hoboken, 2008).

24 Monkhorst, H. J. & Pack, J. D. *Phys. Rev. B* **13**, 5188 (1976).

25 Bengtsson, L. Dipole correction for surface supercell calculations. *Phys. Rev. B* **59**, 12301 (1999).

26 Momma, K. & Izumi, F. VESTA 3 for three-dimensional visualization of crystal, volumetric and morphology data. *J. Appl. Crystallogr.* **44**, 1272-1276 (2011).

27 Huang, Y.-F., Kooyman, P. J. & Koper, M. T. M. Intermediate stages of electrochemical oxidation of single-crystalline platinum revealed by in situ Raman spectroscopy. *Nat. Commun.* **7**, 12440 (2016).

28 Climent, V., Garc á-Araez, N., Herrero, E. & Feliu, J. Potential of zero total charge of platinum single crystals: A local approach to stepped surfaces vicinal to Pt (111). *Russ. J. Electrochem.* **42**, 1145-1160 (2006).

29 Kolb, M. J., Farber, R. G., Derouin, J., Badan, C., Calle-Vallejo, F., Juurlink, L. B., Killelea, D. R. & Koper, M. T. M. Double-Stranded Water on Stepped Platinum Surfaces. *Phys. Rev. Lett.* **116**, 136101 (2016).

30 Kolb, M. J., Calle-Vallejo, F., Juurlink, L. B. & Koper, M. T. M. Density functional theory study of adsorption of H_2O, H, O, and OH on stepped platinum surfaces. *J. Chem. Phys.* **140**, 134708 (2014).